Model for Chainlength-Dependent Core−Surfactant Interaction in $N(Alkyl)_4Cl$-Stabilized Colloidal Metal Particles Obtained from X-ray Absorption Spectroscopy

H. Modrow* and S. Bucher

Physikalisches Institut der Universität Bonn, D-53115 Bonn, Germany

J. Hormes

Center for Advanced Microstructures and Devices, Baton Rouge, Louisiana 70806

R. Brinkmann and H. Bönnemann

Max-Planck-Institut für Kohlenforschung, D-45466 Mülheim, Germany

Received: July 31, 2002; In Final Form: November 11, 2002

This work investigates in detail the interaction between colloidal core and protection shell for $N(octyl)_4Cl$-stabilized cobalt particles of 2.5 nm average diameter. We have analyzed the electronic and geometric structure of these particles using the X-ray absorption near edge structure (XANES) spectra measured at both Cl and Co K edge as well as the extended X-ray absorption fine structure measured at the Co K edge. The metal XANES data are interpreted based on FEFF8 real space full multiple scattering calculations for a suitable reference system. On the basis of these results, we propose a detailed model describing how the protection shell is anchored to the core of the particle. To show the broad applicability of this model, it is then used on Palladium particles stabilized by the same technique.

I. Introduction

One of the standard techniques which is used to stabilize nanosized metal colloids and clusters consists of providing them with a protection shell. Such particles are of high interest as building blocks for new materials as well as for catalytic applications, which in turn require a detailed understanding of morphology and electronic structure of both the stabilizing surfactant and the stabilized metal core. Whereas a considerable amount of evidence based on X-ray absorption techniques is available on the properties of the "core" of such systems, e.g. refs 1−7, only in few studies, e.g. ref 8, the influence of the protection shell is mentioned. However, a detailed understanding of the metal−surfactant interaction is still missing in most cases although this interaction can be rather strong, as shown in a very recent theoretical work by Larsson et al.[9] Consequently, the changing properties of the metal core as a function of surfactant type and exact preparation route might be only partly understood and partly misinterpreted because of missing knowledge about the influence of the protection shell. In fact, we could show only recently[10] that even a small change in the structure of the protection shell can lead to varying electronic properties of the metal core in the case of $N(alkyl)_4Cl$-stabilized Pd colloids. In this process, we could also establish a completely revised understanding of the structure of the surfactant shell, as in contrast to a previous hypothesis, chlorine is involved in bonding the surfactant to the core. Despite this progress, this result remained dissatisfactory inasmuch as no unique decription of the process responsible for the observed changes could be given on an atomic scale.

The reduction of metal salts with tetraalkylammonium hydrotriorganoborates is a general method for the preparation of metal colloids of elements of groups 6−11 in organic solvents.[11,12] During the colloid formation, the stabilizing tetraalkylammonium salts are formed, directly at the reduction center, and act as powerful protecting agents for the metal particles. The resulting colloids can be isolated in a dried state and may be redissolved in various solvents. It turns out that this procedure is successful only for certain alkyl chain lengths for a given metal, which supports the idea that the bonding to the metal core and stability of the resulting colloidal particle is influenced by the chain length. Whereas it seems easy to explain the presence of a lower limit of the chain length, using the simple argument that the efficiency of protection decreases with decreasing length of the (unbranched) *n*-alkyl-chain which leads to a reduced intertwining of these organic groups, it is more difficult to explain the presence of the upper limit. A rather notorious case in this context is the cobalt particles discussed in this study. Despite several tries under varying conditions, it was impossible to stabilize the cobalt colloid using either shorter (hexyl) or longer (decyl) *n*-alkyl chains. Consequently, we have extended our studies to this new system which also offers the chance to gain additional structural information by application of EXAFS. In general, XANES contains detailed information about the absorbing atom, for example about the oxidation state and the effective charge of the element in different compounds,[13] about coordination geometries,[14,15] and about different bonding types.[16] This information can be extracted using "fingerprint" techniques, i.e., by comparing the measured spectra of the substance under investigation to the spectra of well characterized reference compounds. Whereas this approach is used in many studies, the comparison to calculated spectra is often even more instructive, especially if these calculations provide information on the 1-projected density of states as well. Consequently, we have used the real space Green's function code FEFF8[17] to support our investigation by suitable calculations which allow detailed insight into the electronic structure of the samples investigated in this study.

EXAFS spectra can be used to determine the geometry of

* To whom correspondence should be addressed.

10.1021/jp0217740 CCC: $25.00
Published on Web 03/28/2003

the atomic environment of selected absorber atoms quantitatively (e.g., ref 18), yielding radial distances, number, and types of neigboring atoms. In the present context, this method is especially useful, as it does not require long range order of the samples under investigation. Whereas this is often true for small colloidal systems in general, in the present case, we are especially interested in geometric information on the surface of the metal core and the surfactant layer which is in immediate contact with this surface. Because this interface is buried under additional surfactant molecules, this information can be gained with hardly any other technique. Consequently, EXAFS measurements on the Co K edge provide crucial information for our purpose.

Using the experimental and theoretical approaches mentioned above, we can now investigate the problem of core-surfactant interaction in $N(alkyl)_4Cl$-stabilized colloidal metal particles in close detail.

II. Experimental Details

A. Sample Preparation. The colloidal, THF soluble Co nanoparticles investigated in this study were prepared from $CoCl_2$ and tetraalkylammoniumborate, following the reaction

$$CoCl_2 + 2(R)_4NBEt_3H \rightarrow Co_{coll} + 2(R)_4NCl + 2BEt_3 + H_2$$

To vary the chainlength of the *n*-alkyl chains of the protection shell, C_6H_{13}, C_8H_{17}, and $C_{10}H_{21}$, respectively, were used. Following the general procedure described in ref 19, only in the case of C_8H_{17} the color change from blue to deep red-black which is characteristic for the complete reduction of the Cobalt salt was observed. To destroy unconverted reducing agent, abs. acetone was added before filtering off unsoluble material and evaporating all volatile compounds from the clear solution. After drying in a vacuum for 4 h at 40 °C, the Co colloid was obtained in the form of a waxy, deep-black residue. It contains approximately 8 wt % of Co and is extremely soluble in THF, soluble in toluene, acetone, and ether and unsoluble in ethanol and pentane.

To purify the thus obtained material, the whole residue was dissolved in 290 mL of ethanol, and 24 mL of ether was added to precipitate the colloid in form of a light gray-brown powder. After a settling time of at least 1 h, the supernatant solution was pressed off, and the precipitate was washed with a mixture of 50 mL of abs. ethanol and 5 mL of abs. ether. After drying for 16 h in high vacuum, a grayish-black Co colloid powder with a Co content of 51.36 wt % and compact particles with an average size of 2−3 nm (as determined by TEM) was obtained. It is very soluble in THF but unsoluble in toluene, acetone, ether, and ethanol.

In contrast to the successful preparation described above, even with a big excess of reducing agent, it was not possible to achieve the complete reduction described above for the octyl case for either the longer or the shorter alkyl chain, as indicated by the deep green color of the product. This seems to indicate a delicate dependency of the surfactants ability to connect successfully to the Co nanoparticle on the length of the *n*-alkyl chain, which is analyzed in detail in this study.

B. X-ray Absorption Spectroscopy. X-ray absorption measurements were performed at beamline BN3 of the Electron Stretcher and Accelerator ELSA at Bonn University. For the measurements, ELSA was operated at an electron energy of 2.3 GeV and an average electron current of about 35 mA. The synchrotron radiation from ELSA was monochromatized with InSb(111) crystals ($2d = 7.4806$ Å[21]) in a double crystal monochromator of Lemonnier type,[20] yielding a minimum stepwidth of about 0.14 eV at the Cl K edge (2833 eV). At the Co K edge (7709 eV), Ge(220) crystals were used ($2d = 4.00$ Å[21]), leading to a minimal stepwidth of about 0.62 eV.

Balzers QM311 electrometers were employed to read out the current of the ionization chambers used as detection system. These were operated at 200 V, filled with 300 mbar Ar. The electrometers provide an output voltage which is proportional to the ionization current. These voltages were read out using an AD/DA-card of type DT2836 by Data Translation. The photon energy was scanned from at least 40 eV before to 100 eV after the rising edge for the XANES spectra and to 9000 eV for the EXAFS spectra. For each datapoint, an integration time between 200 and 400 ms was used.

To prepare the samples for measurement, the dried colloids were evenly applied to self-adhesive Kapton tape, which results in a colloidal layer of some μm thickness. The preparation took place in a glovebox filled with argon. The sample was transferred to the measuring chamber under argon atmosphere in a special sample holder as well. The optimal sample thickness for the transmission measurement was found by trial and error and was chosen in such a way that the maximum absorption at the corresponding edge μd was not higher than 1.5 to avoid possible thickness effects. Measurements were performed at a temperature of approximately 300 K.

The experimental data were treated as follows: After subtraction of a linear background fitted to the preedge region, the absorption edge is normalized to 1 by dividing by the absorption μd at an energy of 2900 eV at the Cl K edge and at an energy of 7824.6 eV at the Co K edge. The photon energy was calibrated at the Co K edge relative to the pure metal: the first inflection point is set to the binding energy of the 1s electron, 7709 eV.[21] At the Cl K edge, the photon energy calibration is made relative to $PdCl_2$, setting the energy position of the first peak to the binding energy of the 1s electron of pure chlorine, 2833 eV.[21] To evaluate the EXAFS spectra, the UWXAFS program package[22−24] was used. For the fits, which include the *R* range between 1.6 and 3.3 Å, the *k* range 2−12 was used. To test the stability of the fit, k weighting was varied between 1 and 3. The value of S_0^2 was 0.825, as determined by fitting a hcp Co-foil with fixed coordination numbers using identical parameters.

III. Results and Discussion

A. Experimental Observations. We begin our discussion with an analysis of the Co K edge EXAFS data, as the information on the morphology of the particle yields a staunch basis for further interpretation and can validate that the synthesis has in fact produced colloidal metal particles. Figure 1 shows the experimental data as well as the results of the EXAFS analysis, which are also summarized in Table 1. The most important aspect of the EXAFS results is the fact that some chlorine atoms are detected in the environment of cobalt absorber atoms. They are found at a rather long distance from the absorbing atoms, 3.22 Å, whereas a typical distance for a Cl−Co bond is, e.g., 2.51 Å in $CoCl_2$ as derived from the crystallographic data given in ref 25, which suggests that they are coordinated to the surface of the metal particles rather than being embedded into a Co matrix. As the detection of chlorine is of considerable importance for our further analysis, we have included in Table 1 the results of our EXAFS-fits for different *k* weightings, which underline the stability of our results. It should be stressed that a fit using a second Co−Co, a Co−C, or a Co−O scattering path to reproduce this peak fails

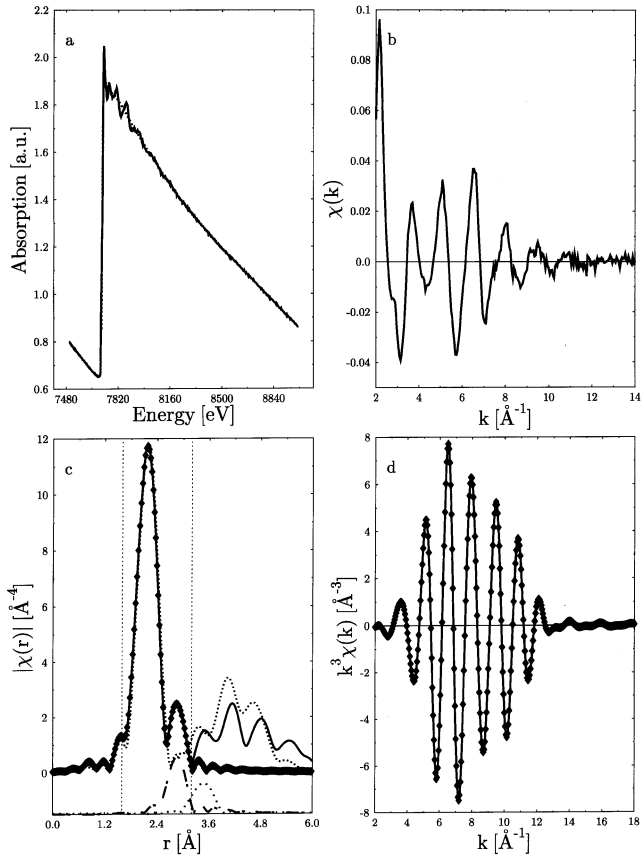

Figure 1. Co K-EXAFS analysis of the tetraoctylammonium-stabilized Co-colloid: (a) raw data (solid) and background (dotted), (b) extracted $\chi(k)$ function, (c) Fourier transformed data in k^3 weighting (solid) in comparison with rescaled Fourier transformed data of Co powder (dotted) and fit (diamonds). To illustrate the small interference between the second shell Co−Co and Co−Cl paths, their respective contributions are also shown (dash and dot) d) data (solid) and fit (diamonds) in q space.

TABLE 1: Results of the EXAFS Analysis of a N(octyl)$_4$Cl-Stabilized Co Colloid for Different *k* Weights (S_0^2=0.825)

k weight	backscatterer	*R*[Å]	*N*	σ^2[Å^2]	E_o [eV]
$k=3$	Co	2.49(1)	4.3(1)	0.008(1)	2.5(3)
	Cl	3.21(1)	1.2(2)	0.004(1)	7.5(1.1)
$k=2$	Co	2.49(1)	4.3(1)	0.008(1)	2.8(3)
	Cl	3.13(3)	1.0(1)	0.003(1)	7.8(1.1)
$k=1$	Co	2.49(1)	4.3(2)	0.007(1)	2.4(4)
	Cl	3.18(2)	1.2(2)	0.001(3)	4.9(1.3)

completely. In fact, it is not at all surprising that no Co−C interaction is visible, whereas the Co−Cl coordination is as follows: apart from the higher scattering amplitude of the heavier Cl atom, the carbon atoms are screened by hydrogen atoms and should thus be expected to contribute at even longer distances, which reduces the amplitudes of their contribution to the EXAFS oszillations further. In addition, the structural order of the chlorine atoms might be significantly higher if they are interacting with the cobalt surface than the one obtained in indirectly interacting long alkyl chains. Furthermore, it turns out that the cobalt atoms present in this sample are mostly surrounded by other cobalt atoms, indicating clearly the presence of small colloidal metal particles and strengthening the hypothesis that the observed Cl-coordination might occur mainly at the surface of the particles. As it is often the case in investigations of metallic nanoparticles,[26−29] a slight reduction of the Co−Co bond length to a value of 2.49 Å is observed. It is interesting to compare the higher coordination shells of the colloidal sample in the $\chi(r)$ function to the ones in cobalt bulk metal (cf Figure 1c). Its principal shape remains almost identical, and a reasonably good fit of these structures can be achieved using higher-shell paths from hcp Co metal, which indicates that in fact several shells of Cobalt are present in the particles we are investigating. It should also be stressed that the overlap between the strong second shell Co−Co path and the Co−Cl path is small (cf. Figure 1c) and that a possible influence of this Co−Co path with the results of the analysis for the Co−Cl path should vary with *k* weighting because of the *k* dependence of the respective scattering amplitudes. Unfortunately, the available number of free parameters for our EXAFS fit is too small to investigate this region using a path-by-path approach which might yield information on the exact nature of deviations from the hcp structure. This is of special interest, as recent literature[30−32] suggests that in Co nanoparticles Co metal atoms might be arranged in fcc, bcc, and/or mixtures thereof or in the β−Mn structure.

Apart from a detailed analysis of the higher coordination shells, the obtained coordination number for the fist Co shell might in principle be used to distinguish between different nanocrystalline Co phases. It is evident that the theoretical coordination number of 12 differs considerably from the value of 4.3 obtained in our fit. For an ideal 2.5 nm, i.e., roughly 5-shell, hcp Co particle, the contribution of surface atoms with a reduced number of nearest neighbors explains a reduction of the average coordination number by about 25% to a value of 9. The significantly smaller coordination number obtained in our study is in better agreement with a bcc structure (8 nearest neighbors reduced to 6 if accounting for surface effects) or a β−Mn structure. It should be noted that a bcc Co structure would require a Co−Co distance of 2.87 Å, which is not in agreement with our anaysis. However, each of these estimates assumes the presence of perfect particles and perfect particle surfaces, which might not be an adequate description for the situation considering, e.g., the results obtained in ref 9. A similar approach for the explanation of drastically reduced coordination numbers obtained when analyzing Fe nanoparticles has been suggested, for example, by Di Cicco et al.[33,34] Another observation when looking at the results of our fit is that, despite the surface relaxation which causes the slight reduction of the Co−Co distance, the fitting result for the Debye−Waller(DW) factor is almost equal to the one observed for cobalt metal (0.0076: 0.0068), whereas it appears physically reasonable to expect a significantly increased value for this parameter and thus a significantly increased value for the coordination number, which is closely correlated to the DW factor. The reason for this rather unphysical result from the fit might be attributed to the Gaussian pair distribution function which is the basis for the inclusion of the effective pair distribution in the DW factor. This assumption is clearly wrong in the present case, as the minimal distance is encountered between the contracted outer two shells of these particles which contain 75% of the cobalt atoms in the particles and the maximal distance between the third and fourth shell, which contain roughly 50% of the cobalt atoms in the particles. Consequently, one might a bond-length distribution which is shaped as an unsymmetric double-well potential and thus far from the Gaussian ideal. As a matter of fact, Babanov et al.[35] have performed a more general EXAFS analysis on Co nanoparticles and reached the conclusion that in a boundary layer of the particles a four-fold coordination might be observed. Apart from an asymmetric static radial distribution function

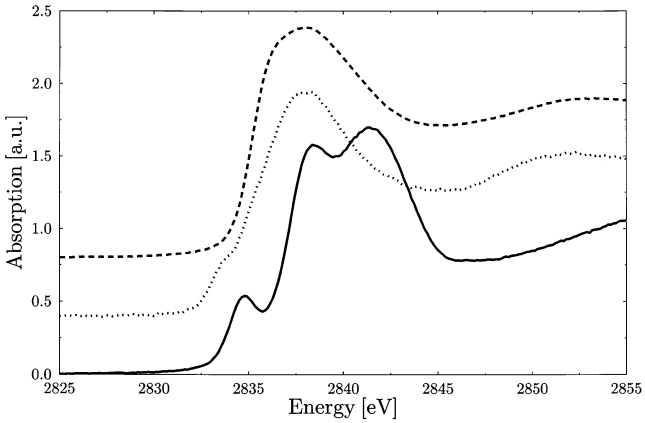

Figure 2. Cl K-XANES spectra of $CoCl_2$ (solid, bottom), tetraoctylammonium-stabilized Co colloid (dotted, middle), and tetraalkylammoniumchloride (dash, top).

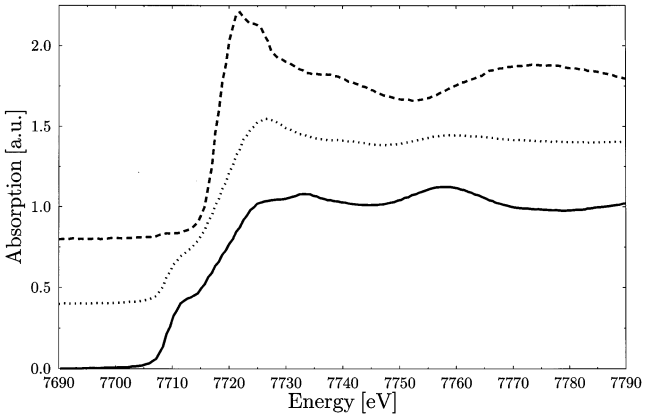

Figure 3. 3. Co K-XANES spectra of Co powder (solid, bottom), tetraoctylammonium-stabilized Co-colloid (dotted, middle), and $CoCl_2$ (dash, top).

discussed in ref 35, anharmonic Co−Co vibrations could lead to a dynamic asymmetry in this function, as discussed in detail in ref 36.

Summing up the EXAFS results, these indicate that we are dealing with compact Co metal nanoparticles, without giving conclusive evidence for the phase they are in. At relatively high distances, a Co−Cl coordination is observed for some of the absorbing Co particles which suggests a surface coordination of the metal by Cl.

The next question which arises is whether the coordination of the Cobalt core to the chlorine will influence the electronic structure in this system despite the rather large distance between these types of atoms. Such an influence on the chlorine can be confirmed immediately when looking at the Cl K-XANES data displayed, in Figure 2. Comparing the spectrum of the $N(octyl)_4Cl$-stabilized cobalt particles to the spectrum obtained from pure $N(octyl)_4Cl$, it is evident that an additional shoulder appears in the spectrum, shifting the first rise of the edge to considerably lower energies. At the same time, one can confirm by direct comparison with the spectrum of $CoCl_2$ that this effect is not due to a contribution of this educt, as the different energy position of the shoulder in the spectra of $N(octyl)_4Cl$-stabilized cobalt particles and $CoCl_2$, respectively, shows. The presence of an additional low-energy structure in the X-ray aborption spectrum is not found in situations in which the chlorine bond is purely ionic, such as the ones described in ref 37, but rather typical for the presence of (covalent) bonds between chlorine and 3d metals.[38−40] Before interpreting this observation further, let us have a look at the electronic structure of the supposed interaction partner, cobalt. In fact, the cobalt K edge spectra displayed in Figure 3 show clear differences between Co powder and the colloidal cobalt particles. Apart from the clear reduction of the intensity of the resonances in the energy region above ≈7745 eV which is typical for the reduction of particle size, one observes significant changes in the white line region, namely, an increase of the white line and a decrease of the low energy shoulder in the absorption spectrum compared to the cobalt powder. In $CoCl_2$, the same trends are observable, but in a much stronger form, whereas especially the corresponding behavior in the white line region is not significantly present in the spectrum of an aluminum-organically stabilized colloidal cobalt particle[11] which has been stabilized using another type of surfactant. Consequently, we can in fact exclude that a particle size effect causes the changes in the whiteline region and attribute the observed changes in the colloid-spectra to an interaction between cobalt and chlorine atoms.

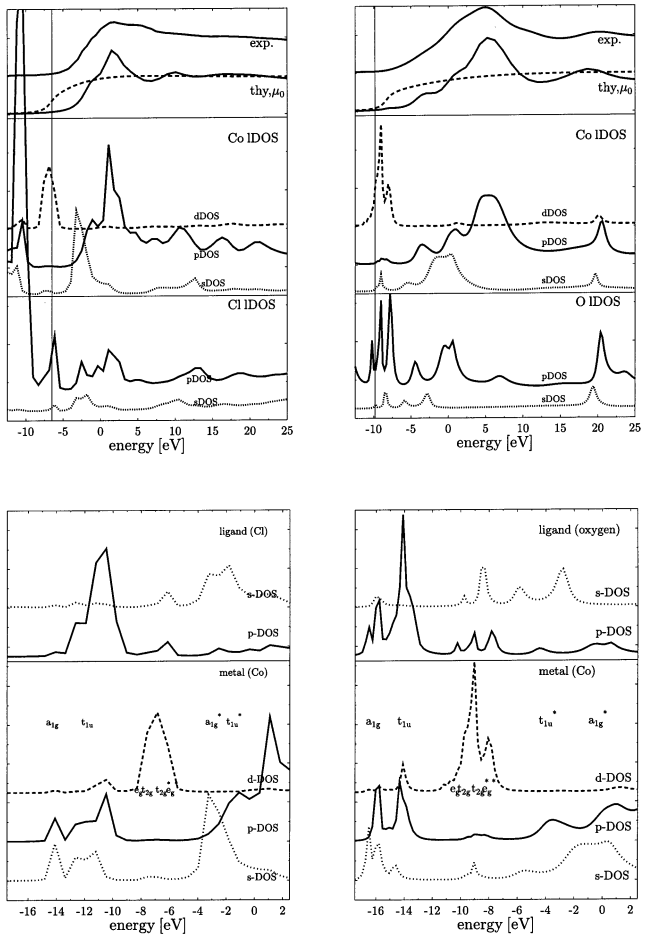

Figure 4. 4. Results of Feff8 calculations on $CoCl_2$ (a,c) and CoO (b,d). In (a) and (b), experiment, theory, and 1- and atom-projected DOS are shown. In (c) and (d), the lDOS is analyzed in terms of ligand field theory.

B. Theoretical Considerations. To gain additional understanding of these observations, FEFF8 calculations on reference materials provide essential information. We shall at first analyze the electronic structure of $CoCl_2$ in comparison to the electronic structure of CoO, as such a comparison elucidates special features of the Co−Cl bond. Figure 4, parts a and b, show the results of the calculations in comparison to experimental data. Evidently, good agreement between theory and experiment is reached in the calculations, making these a solid basis of our further argumentation. In this context, it is especially interesting

TABLE 2: 1-Projected Charge Counts for $CoCl_2$ and CoO Obtained by FEFF8 Calculations

1-projected valence charge	$CoCl_2$	CoO
Co s	0.471	0.465
Co p	0.592	0.627
Co d	7.945	7.740
Cl s/O s	1.943	1.841
Cl p/O p	4.902	4.241

to compare the occupation numbers of the valence shell calculated by FEFF8 for $CoCl_2$ and CoO presented in Table 2, as these show the typical bonding mechanism of the Co−Cl bond as compared to a Co−O bond. Whereas these numbers bear an intrinsic model-imposed systematic error; their direct comparison can be used to derive some trends in the electron configuration. In both cases, the Cobalt atoms with a formal valency of +II are embedded in an octahedral environment formed by the ligands. It should be noted that this embedding is clearly reflected in the 1- and atom-projected density of state plots shown in Figure 4, parts c and d, to which the well-known orbital scheme of ligand-field splitting in an octahedral environment can be applied directly.

This environment causes a significant reduction of valence s charge because of the sp^3d^2 hybridization expected for such a configuration. But it is evident that in the case of $CoCl_2$, the p valence charge which stems from the hybridization process is reduced significantly stronger than in the case of CoO. At the same time, the amount of d valence charge counts is significantly higher in the first case. This suggests the presence of a strong σ-bonding−π-back-bonding effect, which is also supported by the fact that the Co−Cl bond length is significantly larger than the Co−O bond length. These arguments based on the analysis of the charge distribution are fully supported by the corresponding 1-dos calculations. The sp^3d^2 hybridization which is occurring at the Cobalt atom and leads to the formation of six σ-type bonds is clearly reflected in Figure 4. The π-back-bonding can be recognized by the rather significant overlap between Co d-dos and Cl p-dos close to the Fermi-energy. On the basis of this binding mechanism, it is now possible to conclude why the low energy shoulder of the absorption edge observed in the Cl K edge spectra of the $N(octyl)_4Cl$-stabilized Co colloid is shifted relative to the energy position of this structure in $CoCl_2$. In $CoCl_2$, one can assume that the "optimal" Co−Cl bond has been formed; that is, the best possible overlap of atomic orbitals between the bonding partners has been reached, which corresponds to a given energy splitting between bonding and antibonding molecular orbital on one hand and a position in the minimum of the Morse potential which is commonly used to characterize the dependence of the energy of a chemical bond on the other hand (cf Figure 5). We know from the EXAFS analysis of our colloids that the Co−Cl distance is considerably larger than one would expect for a typical Co−Cl bond. As a consequence, the overlap of the atomic orbitals is reduced or might even become zero and the chlorine atom takes the corresponding position on the Morse potential curve (cf Figure 5 left/right column). If this overlap is reduced, the splitting is also reduced between the energy of bonding and antibonding molecular orbital, as schematically shown in the central column of Figure 5, and as the XANES spectra in this electron-rich system are related to the probing antibonding states, this leads to a decreased energy position of the shoulder of the absorption edge in these spectra. What remains to be explained is the observed dislocation of the chlorine atom in the colloidal sample from its optimum position with respect to the Co−Cl bond as encountered, for example, in $CoCl_2$. To understand this effect,

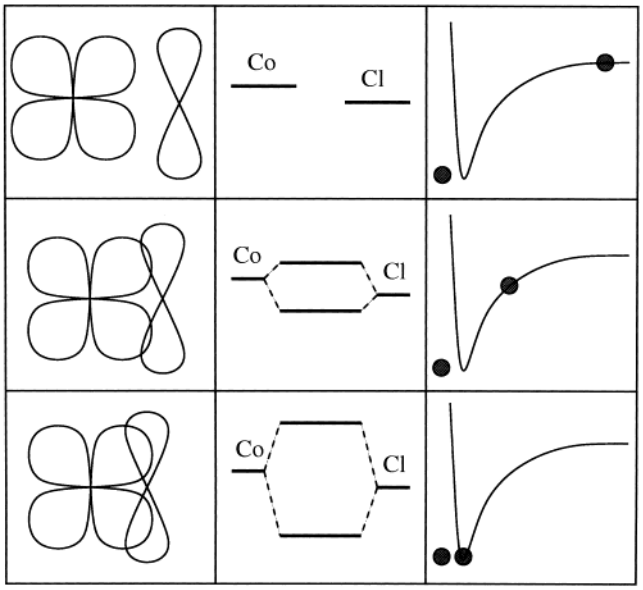

Figure 5. 5. Scheme for the visualization of the bonding situation between Co and Cl in terms of an orbital diagram (left), (b) a state diagram (middle) and (c) a potential curve (right).

one has to remember that in pure $N(octyl)_4Cl$ the Cl and the $N(octyl)_4$ group both bear strong ionic character. From electrostatic considerations, this leads to a more or less tetrahedral configuration of the alkyl groups on which the positive charge of the ion is rather evenly distributed, which in turn defines a sterically enforced minimum distance between the center of this ion and the surface of the colloid. Consequently, apart from the morse potential which approximates the effect of the chemical bonding process as a function of the distance between colloidal cobalt and chlorine, a coulomb potential which represents the attractive force between the counterions is involved in this physical scenario, and the balance of these two forces defines the actual position of the chlorine atom and thus the possible overlap between the atomic orbitals of cobalt and chlorine. It is possible to transfer this argumentation directly to the equally stabilized Palladium colloids. When doing so, our argumentation is not limited to the explanation of the relative peak positions of $PdCl_2$ and the colloidal system as encountered in the Cl K-XANES spectra shown in Figure 6, but yields also an explanation why the energy of the Pd−Cl interaction peaks is shifted relative to the one of the Co−Cl-interaction. Because of the larger number of d electrons of Palladium and the more diffuse nature of the 4d valence orbital of Pd compared to the 3d valence orbital of Co, naturally the overlap which can be established is smaller in the case of Pd. As a consequence, again the antibonding molecular orbital is found shifted to lower energies. As published previously,[10] the energy position of the Pd−Cl resonance in the butyl-stabilized Pd colloid was found at slightly higher energies than the one in the octyl-stabilized system. This fact, which could not be explained in the previous paper, is to be expected in the framework of our new model, as the shorter butyl chain allows for a better optimization of the Pd−Cl bond. However, only a tentative explanation for the stabilization of the butyl system in the case of Pd can be given: Bearing in mind that the Pauling electronegativity of Pd (2.2) is higher than the one of Co (1.8), the interaction with a Cl^- ion will be stronger. This is also reflected in the relatively short Pd−Cl bond length of 2.3 Å in $PdCl_2$. Note that as the energetically less favorable p-orbitals contribute more strongly to the formation of this bond and much weaker back-bonding effects are present due to the increased d-occupation number,

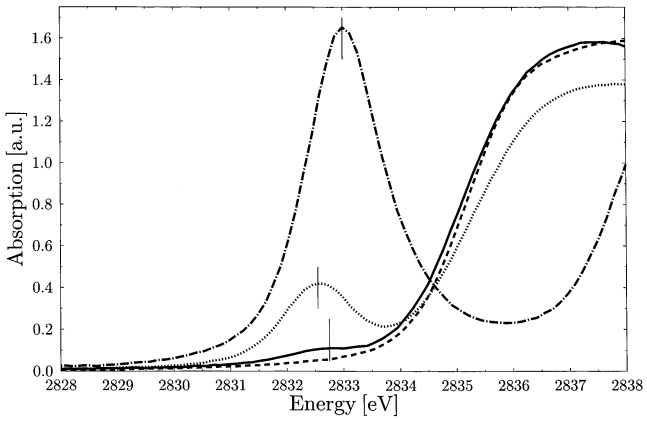

Figure 6. 6. Cl K edge XANES data of tetraalkylammoniumchloride (dash), tetrabutylammonium-stabilized Pd-colloid (solid), tetraoctylammonium-stabilized Pd colloid (dot), and $PdCl_2$ (dash and dot). Intensity differences between the preedge resonances for the two colloid samples are partly due to a different degree of purification.

this is still in agreement with the shift of the Pd−Cl resonance to lower energy. As a consequence of the shortened equilibrium distance, one might assume that this leads to a decreased distance of the entire $N(alkyl)_4^+$ ion to the surface of the Pd particle, which in turn would enforce an enhanced spreading of the alkyl groups, which increases the area a single group covers and the itertwining of such groups. Furthermore, our considerations explain in a natural way why there is an upper limit to the alkylchainlength which can be used to stabilize the colloid: Too long alkyl chains may enforce a long core-Cl distance which is then located in the flat part of the Morse potential. As a consequence, the protection shell is no longer anchored to the metal core but just floating around it.

IV. Conclusions

Using the experimental and theoretical results discussed above, we are able to present a detailed model of the protection shell of $N(alkyl)_4Cl$ stabilized colloidal particles. In this system, chlorine atoms form an interstitial layer between the metal core and the surfactant shell. These atoms form a "conventional" ionic bond to the $N(alkyl)^+$ groups which ensure the effectivity of the protecting cover. Simultaneously, they are anchored to the metal core in these systems by a "backbonding effect" between fully occupied Cl p states and empty transition metal d states. Electrostatic considerations suggest a tetrahedral configuration of the alkyl groups in the $N(alkyl)^+$ ion. Consequently, for steric reasons, there is a minimum distance between metal core and the nitrogen central atoms of this surfactant group which is different for different alkyl chainlengths. The interstitial chlorine ion is subject to an attractive electrostatic force toward the $N(alkyl)^+$ counterion, which dislocates it from the equilibrium position typical for a Co−Cl bond, thus explaining the rather large distance between core and Cl atoms observed in the EXAFS analysis. Consequently, a dependence of the metal−chlorine interaction on the alkyl chainlength is obvious. In the case of very long chains, the Cl can be screened by the alkyl groups and its distance to the metal core gets too large to form any kind of bond. In the case of very short chains, the protection shell is no longer effective, thus preventing the formation of colloidal metal particles. In addition to that, repulsive interactions between different chlorine ions no longer separated by alkyl groups might prevent the formation of the metal−chlorine bond. Consequently, in both cases, the colloidal particles can fail to be stabilized.

Acknowledgment. This work was supported by the DFG within priority program 1072 under Contract Numbers Ho887/7-3 and Bo1135 /3-4.

References and Notes

(1) Harada, M.; Asakura, K.; Ueki, Y.; Toshima, N. *J. Phys. Chem.* **1992**, *96*, 9730.
(2) Franke, R.; Rothe, J.; Becker, R.; Pollmann, J.; Hormes, J.; Bönnemann, H.; Brijoux, W.; Köppler, R. *Adv. Mater.* **1997**, *10*, 126.
(3) Franke, R.; Rothe, J.; Pollmann, J.; Hormes, J.; Bönnemann, H.; Brijoux, W.; Hindenburg, Th. *J. Am. Chem. Soc.* **1996**, *118*, 12090.
(4) Cimini, F.; Prins, R. *J. Phys. Chem. B* **1997**, *101*, 5277.
(5) Cimini, F.; Prins, R. *J. Phys. Chem. B* **1997**, *101*, 5285.
(6) Nashner, M. S.; Frenkel, A. I.; Somerville, D.; Hills, C. W.; Shapley, J. R.; Nuzzo, R. G. *J. Am. Chem. Soc.* **1998**, *120*, 8093.
(7) Wu, Z.; Zhang, J.; Benfield, R. E.; Ding, Y.; Grandjean, D.; Zhang, Z.; Ju, X. *J. Phys. Chem. B* **2002**, *106*, 4569.
(8) Kataby, G.; Koltypin, Yu.; Rothe, J.; Hormes, J.; Felner, I.; Cao, X.; Gedanken, A. *Thin Solid Films* **1998**, *333*, 41.
(9) Larsson, J. A.; Nolan, M.; Green, J. C. *J. Phys. Chem. B* **2002**, *106*, 5831.
(10) Bucher, S.; Hormes, J.; Modrow, H.; Brinkmann, R.; Waldöfner, N.; Bönnemann, H.; Beuermann, L.; Krischok, S.; Maus-Friedrichs, W.; Kempter, V. *Surf. Sci.* **2002**, *497*, 321.
(11) Bönnemann, H.; Brijoux, W.; Brinkmann, R.; Dinjus, E.; Joussen, Th.; Korall, B. *Angew. Chem., Int. Ed. Engl.* **1991**, *30*, 1312.
(12) Bönnemann, H.; Brijoux, W.; Brinkmann, R. *J. Mol. Catal.* **1994**, *86*, 129.
(13) Iwanowski, R. J.; Lawniczak-Jablonska, K. *Acta Phys. Pol. A* **1997**, *97*, 803.
(14) Wong, J.; Lytle, F. W.; Messmer, R. P.; Maylotte, D. H. *Phys. Rev. B* **1984**, *30*, 5596.
(15) Verdaguer, M.; Briois, V.; Cartier, C.; Gadet, V.; Michalowicz, A. *2nd Conference on Progress in X-Ray Synchrotron Radiation Research*; Conference Proceedings Vol. 25; SIF: Bologna, 1990; p 889.
(16) Behrens, P. *Trends Anal. Chem.* **1992**, *11*, 237.
(17) Ankudinov, A.; Ravel, B.; Rehr, J. J.; Conradson, S. *Phys. Rev. B* **1998**, *58*, 7565.
(18) B. K. *Teo: EXAFS: Basic principles and data analysis*, *Inorganic Chemistry Concepts*; Springer: Berlin, 1986; Vol. 9.
(19) Bönnemann, H.; Richards, R. M. *Eur. J. Inorg. Chem.* **2001**, 2455.
(20) Lemonnier, M.; Collet, O.; Depautex, C.; Esteva, J. M.; Raoux, D. *Nucl. Instr. Methods A* **1978**, *152*, 109.
(21) Vaughan, D., Ed.; *X-ray Data Booklet*; Lawrence Berkeley Laboratory, University of Califonia: Berkeley, CA, 1986.
(22) Stern, E. A.; Newville, M.; Yacopby, Y.; Haskel, D. *Physica B* **1995**, *209*, 117.
(23) Newville, M.; Livins, P.; Yacoby, Y.; Rehr, J. J.; Stern, E. A. *Phys. Rev. B* **1993**, *47*, 14126.
(24) Newville, M.; Ravel, B.; Haskel, D.; Stern, E. A.; Yacoby, Y. *Physica B* **1995**, *209*, 154.
(25) Grime, H.; Santos, J. A. *Z. Kristallgeometrie, Kristallphys,, Kristallchem.* **1934**, *88*, 136.
(26) Balerna, A.; Bernieri, E.; Picozzi, P.; Reale, A.; Santucci, S.; Burattini, E.; Mobilio, S. *Surf. Sci.* **1985**, *156*, 206.
(27) Fairbanks, M. C.; Benfield, R. E.; Newport, R. J.; Schmid, G. *Solid State Commun.* **1990**, *73*, 299.
(28) Benfield, R. E.; Filipponi, A.; Bowron, D. T.; Newport, R. J.; Gurman, S. J.; Schmid, G. *Physica B* **1995**, *208−209*, 671.
(29) Benfield, R. E.; Filipponi, A.; Morgante, N.; Schmid, G. *J. Organometallic Chem.* **1999**, *573*, 299.
(30) Sun, S.; Murray, C. B. *J. Appl. Phys.* **1999**, *85*, 4325.
(31) Puntes, V. F.; Krishnan, K. M.; Alivisatos, P. *Appl. Phys. Lett.* **2001**, *78*, 2187.
(32) Guirado-Lopez, R.; Aguiilera-Granja, F.; Montejano-Carrizales, J. M. *Phys. Rev. B* **2002**, *65*, 045420.
(33) Di Cicco, A.; Berrettoni, M.; Stiza, S.; Bonetti, E.; Cocco, G. *Phys. Rev. B* **1994**, *50*, 12386.
(34) Di Cicco, A.; Berrettoni, M.; Stiza, S.; Bonetti, E. *Physica B* **1995**, *208−209*, 547.
(35) Babanov, Y. A.; Golovshchikova, I. V.; Boscherini, F.; Haubold, T.; Mobilio, S. *Nucl. Instrum. Methods A* **1995**, *359*, 231.
(36) Clausen, B. S.; Norskov, J. N. *Top. Catal.* **2000**, *10*, 221.
(37) Huggins, F. E.; Huffman, G. P. *Fuel* **1995**, *74*, 556.
(38) Rompel, A.; Andrews, J. C.; Cinco, R. M.; Wemple, W.; Christou, G.; Law, N. A.; Pecocaro, V. L.; Sauer, K.; Yachandra, V. K.; Klein, M. P. *J. Am. Chem. Soc.* **1997**, *119*, 4465.
(39) Shadle, S. E.; Hedman, B.; Hodgson, K. O.; Solomon, E. I. *J. Am. Chem. Soc.* **1995**, *117*, 2259.
(40) Hedman, B.; Hodgson, K. O.; Solomon, E. I. *J. Am. Chem. Soc.* **1990**, *112*, 1643.